MULTI-SENSOR ACOUSTIC EMISSION ANALYSIS TOWARDS THE STUDY OF OXIDE-BASED CERAMIC MATRIX COMPOSITES DAMAGE BEHAVIOR

Nicolas Guel[1,2,3], Nathalie Godin[2], Olivier Caty[3], Pascal Reynaud[2], Florent Bouillon[4] and Stéphane Mahdi[1]

[1] IRT Saint-Exupéry, 7 Esplanade des Arts et Métiers, 33405 Talence Cedex, France
Email: nicolas.guel@irt-saintexupery.com, stephane.mahdi@irt-saintexupery.com,
Web Page: http://www.irt-saintexupery.com
[2] Université de Lyon, INSA de Lyon, MATEIS, CNRS UMR-5510, 7 avenue Jean Capelle, 69621 Villeurbanne Cedex, France
Email: nathalie.godin@insa-lyon.fr, pascal.reynaud@insa-lyon.fr,
Web Page: http://www.mateis.insa-lyon.fr
[3] LCTS CNRS UMR-5801, Université de Bordeaux, 3 allée de la Boétie, 33600 Pessac, France
Email: caty@lcts.u-bordeaux.fr,
Web Page: http://www.lcts.u-bordeaux.fr
[4] Safran Ceramics, Rue de Touban, 33185 Le Haillan, France
Email: florent.bouillon@safrangroup.com,
Web Page: https://www.safran-group.com

Keywords: CMC, Damage Mechanisms, Acoustic Emission, In-situ testing, Mechanical Behavior

Abstract
Oxide-based Ceramic Matrix Composites (CMCs) are good candidate materials for new generation of civil aircraft engines. Their excellent thermomechanical properties combined with a low density make them suitable to fulfill hot component requirements. The manufactory process generates several kinds of heterogeneities at different scales in the material (macroporosity, shrinkage cracks, microporosity…). In this study, damage kinetics of the material is inspected through acoustic emission (AE) analysis and in-situ mechanical tests. Several damage mechanisms are detected through X-Ray synchrotron computed µ-tomography and SEM in-situ tests: matrix cracks, fiber-matrix debonding and delamination. Macroscopic mechanical tests were monitored with two kinds of resonant sensors operating in different frequency range. AE signal data fusion limits device-dependent acoustic information. Merged data lead to consistent signal clustering. These clusters are linked with damage mechanisms thanks to in-situ observations.

1. Introduction

Oxide-based CMCs exhibits better thermomechanical properties and lower density than metals. In parallel of high-performance/high-cost SiC-based CMCs, these materials are developed in order to replace metallic rear parts of engines. Recent developments lead aircraft engine companies to build oxide-based CMCs demonstrators. However, certification procedure requires proper understanding of damage behavior.

Processing route generates various heterogeneities such as macroporosity, shrinkage cracks, intra-tow porosity and microporosity. Only few papers describe oxide-based CMCs damage scenarii [1,2] and even less takes into account heterogeneities [3]. The aim of this paper is to establish a relationship

between the microstructure and the mechanical behavior of bidimensional composite. Damage mechanisms inspection is performed with acoustic emission (AE) and in-situ mechanical tests.

Acoustic emission allows real time damage monitoring. AE signals are generated from the release of energy originating at sources located within the materials. Damage kinetics can be associate with the number or the energy of activated sources [4]. Another approach is based on signal waveform characterization. Several descriptors are calculated from each waveform to associate signals with similar characteristics. Algorithms derived from shape detection regroup similar signals into classes [2,5]. Damage mechanisms can be link with signal classes thanks to microstructural observations. Most of the time, acoustic emission is collected from resonant sensor due to their good sensibility. However, frequency content is modified with resonant sensor [6]. Waveform characterization is strongly dependent on sensor features. Information from two kinds of resonant sensors with complementary frequency range is considered in this paper to reduce device dependent results. Data from the two sensors were fused in order to have global information of each source.

This technique was applied on bidimensional oxide composites tensile tests, named macroscopic tests throughout the rest of the document. Mechanical properties in 0/90° and ±45° orientation were determined in this study. This paper will only consider 0/90° tensile tests. Signal classification was achieved with principal component analysis (PCA) and k-means clustering optimized by genetic algorithm [7]. Signal cluster labelling was realized with in-situ tensile tests. Microstructural damage visualization was performed through X-ray synchrotron computed µ-tomography (µCT) and scanning electron microscopy (SEM).

2. Materials and Test Procedures

2.1. Materials

Tested oxide-based CMC contains alumina fibers (Nextel™610 – 3M) regrouped into tows and microporous aluminosilicate matrix obtained by sintering. Microporosity allows crack deviation in fiber-matrix interfaces and therefore nonlinear mechanical behavior [8]. Considered composite is made of 12 plies with 8-harness satin weaving. The final structure $[0/90]_{6S}$ have a fiber volume fraction included between 45% and 50%. Microstructure analysis shows macroporosity, shrinkage cracks and intra-tow porosity (Fig. 1). Dog-bone samples were extracted from 2.5 mm thickness composite plates. Specimen with a gauge length of 30 mm and a gauge width of 16 mm were studied during macroscopic tensile tests. In-situ tensile test specimen have lower gauge dimension (length of 10 mm and width of 4 mm).

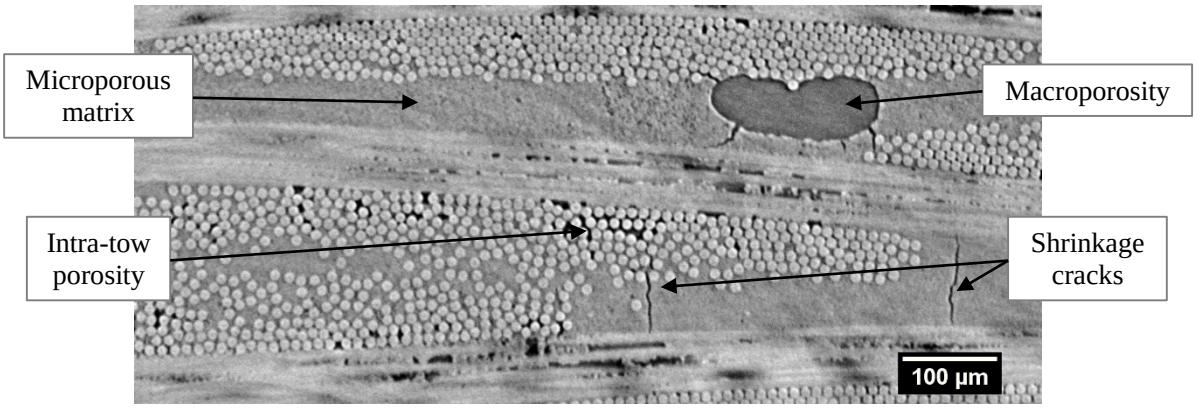

Figure 1. Typical microstructure of Nextel™610/aluminosilicate oxide CMC; X-ray synchrotron 2D tomographic reconstruction

2.2. Test Procedures

Mechanical tests were performed in three different scales: macroscopic scale with multi-sensor acoustic emission monitoring, mesoscopic domain through X-ray synchrotron µCT and microscopic range with SEM.

2.2.1. Macroscopic test procedure

Monotonic and cyclic tensile tests were carried out at room temperature using MTS 610 hydraulic testing machine. Considering oxide CMCs mechanical properties and proper AE recording, displacement speed was set to 0.05 mm.min^{-1}. Longitudinal strains were measured with a 25 mm gauge length extensometer. AE activity were monitored using 2 kind of resonant transducers: Mistras Nano30 (frequency range: 125-750 kHz) and Mistras PicoHF (frequency range: 500-1850 kHz). Two sensors of each kind of transducer were positioned on opposite sides of the sample (Fig. 2). Distance between sensors was set to 50 mm. A value of 40 dB is set for signal pre-amplification. A threshold of 40 dB was applied for each tensile test. AE waveforms were recorded with Mistras PCI2 acquisition system. In accordance with pencil break calibration, wave velocity in the fiber orientation was fixed at 6800 m.s^{-1}. Considering the limited amount of localized sources, this study takes into account localized and non-localized sources.

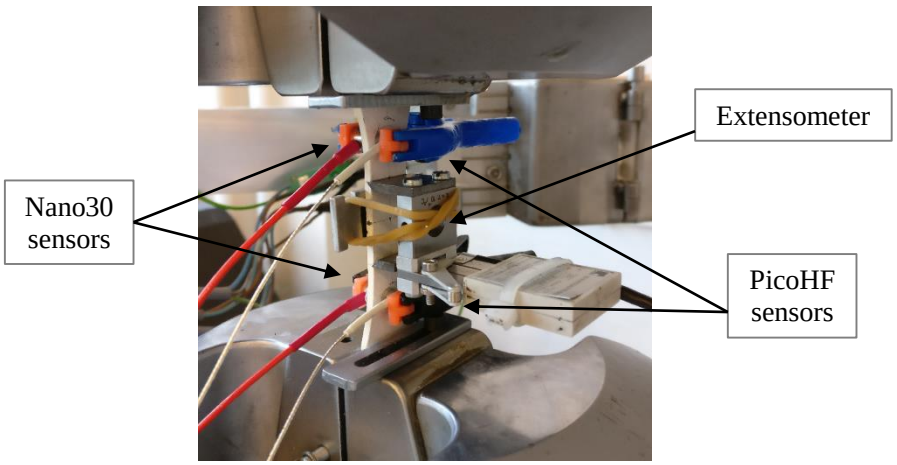

Figure 2. Multi-sensor AE monitoring during macroscopic tensile test

2.2.2. In-situ test procedure

In-situ tensile tests were driven under displacement control. Displacement speed was set to 0.025 mm.min^{-1} in order to have similar strain velocity than macroscopic tests. Microstructure were investigated at several load states until failure of the specimen. Each test were monitored with two Mistras Pico sensor (frequency range: 200-750 kHz). The distance between the sensors was fixed at 25 mm.

In-situ X-ray µCT tensile tests have been carried out on the PSICHE beamline at SOLEIL Synchrotron facility. At each state, 3D volume of the sample gauge were obtained with a voxel size of 2.6 µm. Crack detection is performed with image treatment between initial and deformed states. In-situ SEM tensile tests have been achieved with FEI Quanta 400 FEG environmental SEM. Considering alumina insulator properties, observations were accomplished under environmental mode. Damage kinetics were investigated on polished edge of the sample gauge.

Regarding in-situ sample gauge dimensions, several analysis have been carried out to evaluate the representativeness of in-situ mechanical tests. AE activity and mechanical properties of in-situ samples shows comparable trends than those observed in macroscopic mechanical tests.

2.3. Signal characterization and unsupervised clustering

Waveform preprocessing step is accomplished after EA signal collection. The aim of this step is to remove useless information and improve waveform aspect in order to characterize them. The process stem from previous works [9] and could be decompose in four phases. Consecutively to pre-trigger deletion, tail cutting achieved from an energy criteria to remove the end of the signal: discretized energy of each waveform is determined from temporal sliding window. If the window energy is lower than 0.1% of the cumulative energy from the beginning of the signal, the starting point of the window is considered as the end of the signal. SPI resampling and wavelet denoising are successively performed on waveform. Several descriptors are calculated from preprocessed waveforms in temporal domain and frequency domain thanks to Fast Fourier transform (FFT). Besides conventional descriptors, calculated descriptors have been implemented from former AE analysis on composite materials and corrosion detection [9,10].

Data clustering is carried out from calculated signal characteristics. Uncorrelated descriptors are selected with dendrogram classifier. PCA analysis is applied on selected descriptors to reduce data dimension. K-means clustering optimized by genetic algorithm operates several data partition. The quality of each classification is evaluated thanks to Davies & Bouldin [1] and silhouettes [2] criterion.

3. Results and discussion

All the results are presented in terms of normalized stress σ: stress divided by the ultimate tensile stress observed during macroscopic tensile test.

3.1. In-situ observation

Two in-situ tensile tests (0/90°) under SEM and one through synchrotron have been conducted during this study. Normalized ultimate stress obtained were 0.71, 0.73 and 0.78 respectively for SEM and µCT in-situ tensile tests. Studied oxide-based CMC reveals several damage mechanisms during tensile test such as shrinkage crack opening, intra-tow fiber debonding (Fig. 3.a), tow debonding and crack delamination (Fig. 3.b). The two first cited mechanisms are detected in the early stages ($\sigma = 0.1–0.2$) of the in-situ SEM tensile test. Delamination cracks are observed in the following steps ($\sigma = 0.3–0.75$) with SEM and µCT. Macroporosity seems to initiate delamination throughout the material (Fig. 3.b).

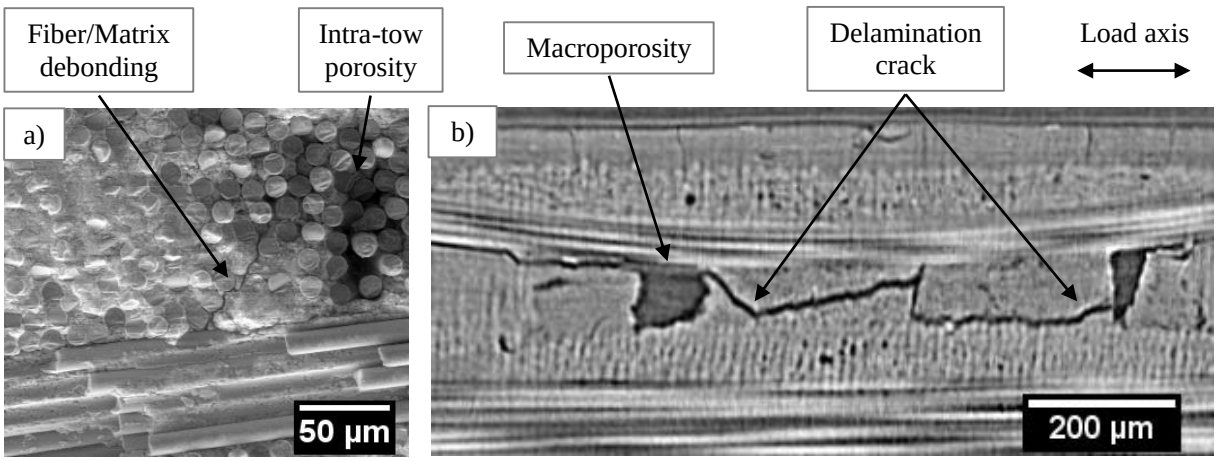

Figure 3. a) SEM observation revealing intra-tow fiber/matrix debonding (σ = 0.2), b) 2D µCT reconstruction showing crack delamination (σ = 0.7)

Localized acoustic emission and µCT crack delamination both contains volumetric information and thus could be compared. High energy localized AE signals are correlated with delamination cracks.

3.2. Acoustic emission analysis

Following AE analysis are based on five macroscopic tensile tests in fiber orientation to guarantee results repeatability. Tensile response is characterized by practically linear behavior with a slight non linearity in stress domain σ = 0.1–0.3 (Fig 4). Studied material exhibits more pronounced damaged behavior close to ultimate stress (σ > 0.9). Nano30 sensors have better signal detection than PicoHF sensors, especially during the first part of the test (Fig. 4.a). Sensor sensibility and frequency content of the sources are investigated. Global AE analysis also reveals the onset of energetic activity during linear behavior (σ = 0.3-0.4) for both sensors (Fig 4.b).

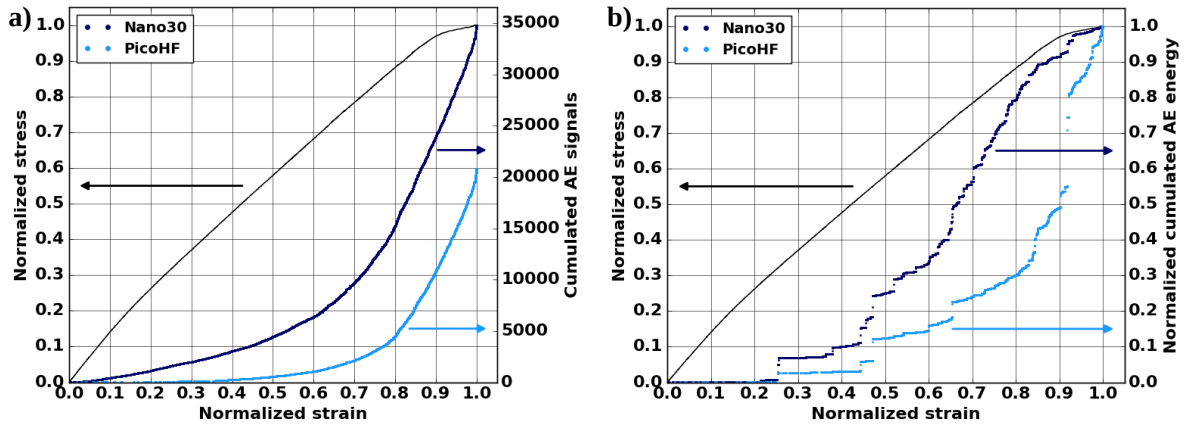

Figure 4. Global AE activity during macroscopic tensile test in fiber orientation obtained from Nano30 and PicoHF sensors; a) Cumulated AE signals, b) Normalized cumulated AE energy

Sources recorded with two kinds of sensors located at the same position along the gauge length are associated using acquisition time. Associated signals represent 80% of the signals recorded with PicoHF sensors. Feature extraction is processed separately for each waveform. Signals characterization exhibits strong differences between Nano30 signals and PicoHF signals. Signals recorded from PicoHF sensors exhibit lower amplitude and higher frequency content than Nano30 signals (Fig. 5).

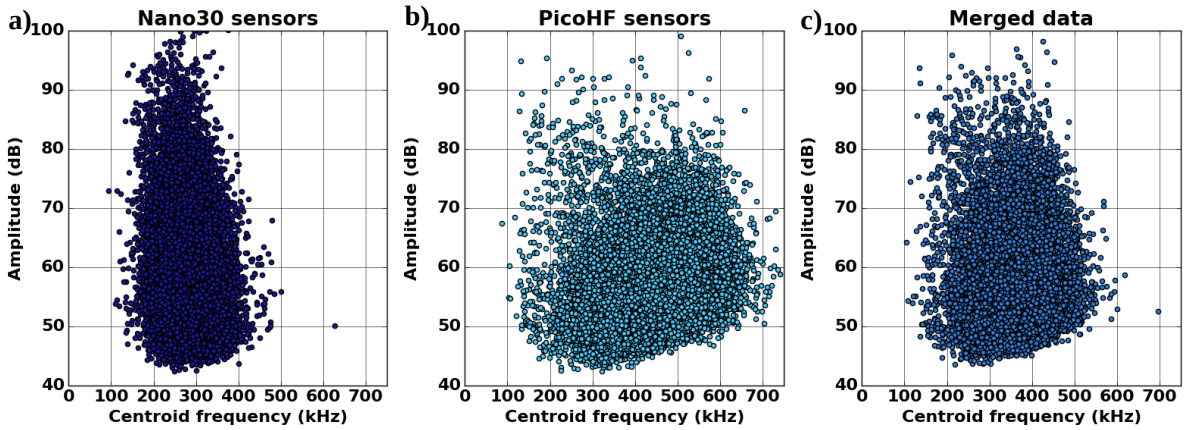

Figure 5. Amplitudes and centroid frequencies calculated from same sources recorded with the two kinds of sensors during a macroscopic tensile test in fiber orientation; a) Nano30 sensors, b) PicoHF sensors, c) Merged data

Complementary information is collected from the two kinds of sensors. Calculated descriptors from both sensors are merged using mean value (Eq. 1). Energetic descriptors are obtained from root mean square (Eq. 2).

$$d^i_{merged} = d^i_{Nano30} + d^i_{PicoHF}/2 \quad (1)$$

$$d^i_{merged} = \sqrt{\left(d^i_{Nano30}{}^2 + d^i_{PicoHF}{}^2\right)/2} \quad (2)$$

d^i_{merged} *: descriptor n°i calculated from the two kinds of sensors*
d^i_{Nano30} *: descriptor n°i calculated from the waveform recorded with Nano30 sensor*
d^i_{PicoHF} *: descriptor n°i calculated from the waveform recorded with PicoHF sensor*

Signal clustering are based on fused descriptors. Seven uncorrelated descriptors are kept to perform PCA and k-means algorithms. Repeatable and well-partitioned classifications are obtained with 4-class partition. Clusters are well-separated in an amplitude-frequency domain (Table 1).

Table 1. Median values of signal cluster descriptors.

Cluster	*Amplitude* (dB)	*Duration* (µs)	*Rise angle* (dB.µs^{-1})	*Centroid frequency* (kHz)	*Spectral spread* (kHz)	*Amplitude/ frequency* (dB.kHz^{-1})
1	56	210	3.7	410	255	0.15
2	55	290	1.6	310	240	0.19
3	71	225	4.9	380	225	0.21
4	66	320	1.6	250	205	0.27

Clusters 3 and 4 contains less than 10% of the total amount of associated signals. Nevertheless, these clusters enclose more than 90% of the cumulated AE energy. Indeed, these signals correspond to critical damage. The onset of energetic activity observed in Fig. 4.b is highly correlated with the appearance of cluster 3 (Fig 5.b). Cluster 4 represent an important part of the AE energy but a small amount these signals are located. The major part of these signals appears for stress level lower than 0.8 (Fig 5.a). Signals with low energy (clusters 1 and 2) become predominant close to the rupture.

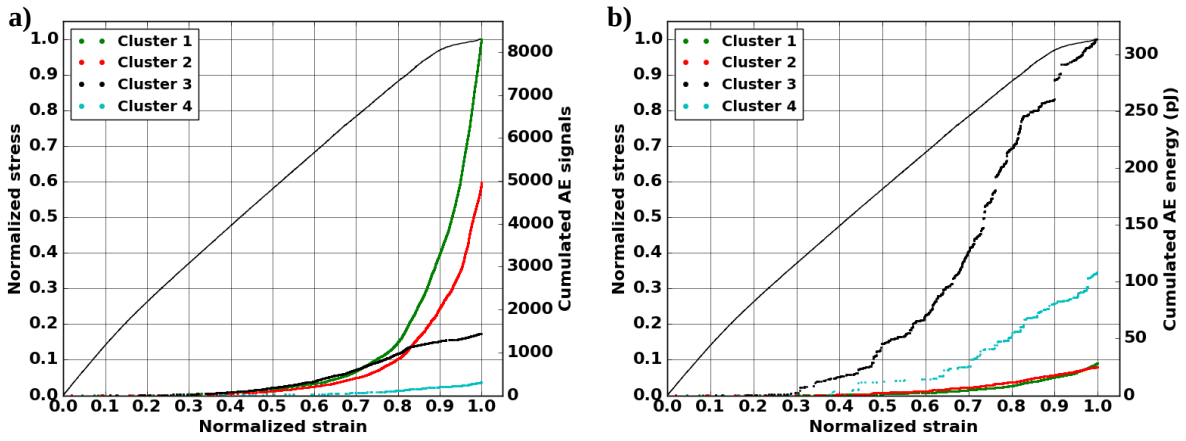

Figure 5. Evolution of AE activity for each cluster during a macroscopic tensile test in fiber orientation; a) Cumulated AE signals, b) Cumulated AE energy

Considering in-situ observations, cluster 3 is associated with delamination cracks. These energetic signals are not correlated with a loss of mechanical properties, reflecting damage longitudinal to the loading axis. Clusters 1 and 2 are linked to lower scale damage such as fiber/matrix debonding and

matrix crack. Fiber failure are inspected to be included in low amplitude cluster. The coalescence of these damage lead to a decrease of mechanical properties then macroscopic failure. Further investigation are necessary to clearly identify the origin of cluster 4. This multi-sensor study allows to separate delamination from the other damage mechanisms. Delamination is the most critical damage in oxide-based CMCs. This damage could not be identify on longitudinal mechanical properties. AE monitoring is an effective technique to prevent damage in these materials.

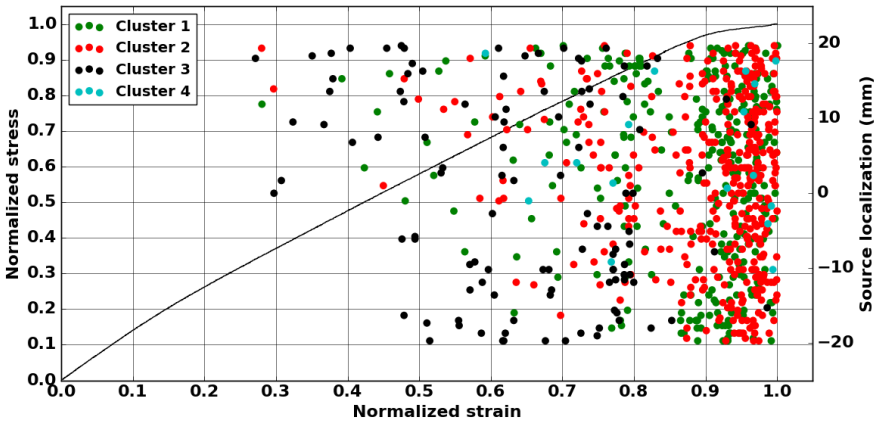

Figure 6. Evolution of localized AE sources for each cluster during a macroscopic tensile test in fiber orientation

The origin of frequency content differences requires a proper understanding of AE sources. Several hypothesis are set to explain frequency partition: influence of propagation media, damage evolution and failure orientation. Further works are required to comprehend the influence these effects on recorded signals. AE modelling seems to be a promising approach to dissociate them [13,14].

Acknowledgments

The authors acknowledge the members of IRT Saint-Exupery collaborative project on oxide composites. This research was realized in IRT Saint-Exupery and funding by the French National Agency for Research (ANR) in collaboration with Safran Ceramics. SOLEIL synchrotron PSICHE beamline team is also acknowledge for their contribution in the µCT in-situ tensile tests experiments.

References

[1] F.W. Zok and C.G. Levi. Mechanical properties of porous-matrix ceramic composites. *Advanced Engineering Materials*, 3:15-23, 2001.

[2] V. Kostopoulos, T. Loutas, A. Kontsos, G. Sotiriadis and Y. Pappas. On the identification of the failure mechanisms in oxide/oxide composites using acoustic emission. *NDT&E International*, 36:571–580, 2003.

[3] C. Ben Ramdane, A. Julian-Jankowiak, R. Valle, Y. Renollet, M. Parlier, E. Martin and P. Diss. Microstructure and mechanical behaviour of a Nextel™610/alumina weak matrix composite subjected to tensile and compressive loadings. *Journal of the European Ceramic Society*, 37(8):2919–2932, 2017.

[4] G.N. Morscher. Stress-dependent matrix cracking in 2D woven SiC-fiber reinforced melt-infiltrated SiC matrix composites. *Composites Science and Technology*, 64(9):1311–1319, 2004.

[5] N. Godin, S. Huguet, R. Gaertner and L. Salmon. Clustering of acoustic emission signals collected during tensile tests on unidirectional glass/polyester composite using supervised and unsupervised classifiers. *NDT&E International*, 37:253–264, 2003.

[6] T. Le Gall, N. Godin, T. Monnier, C. Fusco and Z. Hamam. Acoustic Emission modeling from the source to the detected signal: model validation and identification of relevant descriptors. *Inauguration Conference of International Institute of Innovative Acoustic Emission IIIAE-2016, Kyoto, Japan,* December 5-8 2016.

[7] A. Sibil, N. Godin, M. R'Mili, E. Maillet and G. Fantozzi. Optimization of Acoustic Emission Data Clustering by a Genetic Algorithm Method. *Journal of Nondestructive Evaluation,* 31(2):169–180, 2012.

[8] L. Lange, W.C. Tu and A.G. Evans. Processing of damage-tolerant, oxidation-resistant ceramic matrix composites by a precursor infiltration and pyrolysis method. *Material Science Engineering,* 195:145-150, 1995.

[9] N. Morizet, N. Godin, J. Tang, E. Maillet, M. Fregonese and B. Normand. Classification of acoustic emission signals using wavelets and Random Forests : Application to localized corrosion. *Mechanical Systems and Signal Processing,* 70-71:1026–1037, 2016.

[10] M. Moevus, N. Godin, M. R'Mili, D. Rouby, P. Reynaud, G. Fantozzi and G. Farizy. Analysis of damage mechanisms and associated acoustic emission in two SiC_f/[Si-B-C] composites exhibiting different tensile behaviours. Part II: Unsupervised acoustic emission data clustering. *Composites Science and Technology,* 68(6):1258–1265, 2008.

[11] D.L. Davies and D.W. Bouldin. A Cluster Separation Measure. *IEEE Transactions on Pattern Analysis and Machine Intelligence,* 2:224-227, 1979.

[12] P.J. Rousseeuw. Silhouettes: a graphical aid to the interpretation and validation of cluster analysis. *Journal of computational and applied mathematics,* 20:53-65, 1987.

[13] M.A. Hamstad. Acoustic emission signals generated by monopole (pencil lead break) versus dipole sources: finite element modeling and experiments. *Journal of Acoustic Emission,* 25:92-106, 2007.

[14] M.G.R. Sause and S. Horn. Simulation of Acoustic Emission in Planar Carbon Fiber Reinforced Plastic Specimens. *Journal of Nondestructive Evaluation,* 29:123–142, 2010.